

## TEMPERATURE MODULATION IN RAYLEIGH–BÉNARD CONVECTION

JITENDER SINGH<sup>✉1</sup> and RENU BAJAJ<sup>2</sup>

(Received 1 December, 2008; revised 6 December, 2008)

### Abstract

The stability characteristics of an infinite horizontal fluid layer excited by a time-periodic, sinusoidally varying free-boundary temperature, have been investigated numerically using the Floquet theory. It has been found that the modulation of the temperature gradient across the fluid layer affects the onset of the Rayleigh–Bénard convection. Modulation can give rise to instability in the subcritical conditions and it can also suppress the instability in the supercritical cases. The instability in the fluid layer manifests itself in the form of either a harmonic or subharmonic flow, controlled by thermal modulation.

2000 *Mathematics subject classification*: primary 76D17; secondary 76E07.

*Keywords and phrases*: convection, temperature modulation, parametric instability.

### 1. Introduction

Hydrodynamic systems show a change in flow behavior in response to parametric modulation of driving force. In this regard, Rayleigh–Bénard convection [2, 3, 5, 9] is an interesting and well-studied problem of instability phenomena. External modulation can be produced in the system either by oscillating the container vertically, thereby producing sinusoidal variation of vertical acceleration [7], or by time-periodic heating of the fluid layer. The instability may appear in synchronous or subharmonic mode.

Chen and Chen [4] examined the problem of convection in a vertical infinite slot under gravity modulation. They found that the critical state alternates between synchronous and subharmonic modes. The higher driving frequency tends to suppress the subharmonic oscillations. The instability is shear-dominated for a fluid with Prandtl number 1 and, buoyancy-dominated for a fluid with Prandtl number 25.

<sup>1</sup>Indian Statistical Institute, Kolkata-700108, India; e-mail: [jitender\\_r@isical.ac.in](mailto:jitender_r@isical.ac.in).

<sup>2</sup>Centre for Advanced Study in Mathematics, Panjab University, Chandigarh-160014, India; e-mail: [rbajaj@pu.ac.in](mailto:rbajaj@pu.ac.in).

© Australian Mathematical Society 2009, Serial-fee code 1446-1811/2009 \$16.00

The structural characteristics of convective flows also change with the temperature modulation.

Venezian [14] studied the Rayleigh–Bénard convection with a time-dependent sinusoidal perturbation applied to the wall temperatures. He considered small amplitude of modulation and obtained the shift in the critical Rayleigh number as a function of the driving frequency. He found that it is possible to advance or delay the onset of convection by time modulation of the wall temperatures. Yih and Li [15] investigated the formation of convective cells in a fluid between two horizontal rigid boundaries with time-periodic temperature distribution, using the Floquet theory, for the Prandtl numbers of air (0.73) and water (7.0). They found that with the temperature modulation, convection cells oscillate either synchronously or with half frequency. Rosenblat and Tanaka [13] used the Galerkin method to solve the linear stability problem and obtained the critical temperature gradient at the onset of the modulated convection. They found that the critical Rayleigh number increases with modulation. Roppo *et al.* [12] discussed the Bénard convection with sinusoidal time modulation of the lower wall temperature. Using weakly nonlinear analysis of the flow, they found that the modulation produces a range of stable hexagonal patterns near the critical Rayleigh number. These hexagons bifurcate subcritically and correspond to the fluid flow downwards at the cell centers.

The previous work on convection in a horizontal fluid layer, driven by time-periodically varying temperatures of the boundaries, has emphasized the critical onset of instability by computing the values of the critical Rayleigh number. However, the instability can occur at any value of the temperature difference applied to the boundaries of the fluid layer, and is controlled by the amplitude and frequency of modulation. In the absence of modulation, the fluid layer is stable with respect to small disturbances, for all values of Rayleigh number  $Ra < 657.511$ ; but the modulation can give rise to convection in subcritical conditions. Also, for supercritical conditions ( $Ra > 657.511$ ), the phenomenon of convection can be suppressed by the modulation. We address this issue in the present study. We investigate numerically the effect of time-periodic modulation of the free-boundary temperatures on the onset of Rayleigh–Bénard convection in an infinite, horizontal, Boussinesq fluid layer. The stability analysis is done using Floquet theory [6, 8]. We find that the instability in subcritical and supercritical conditions can set in as harmonic or subharmonic flows, which are controlled by modulation. To see this, the resonance bands in the plane of the dimensionless wavenumber of disturbance and the amplitude of modulation, are obtained for various combinations of the dimensionless parameters. To obtain the resonance bands, we employ the same method as Kumar [10] and Bajaj [1].

## 2. Mathematical formulation

Consider an infinite, horizontal, viscous, Boussinesq fluid layer of thickness  $d$ , whose lower and upper ends are the planes  $z = 0$  and  $z = d$ , respectively. The system

is described by the equations

$$\begin{aligned} \rho_0 \frac{\partial \mathbf{u}}{\partial t} + \rho_0 \mathbf{u} \cdot \nabla \mathbf{u} &= -\nabla p + \eta \nabla^2 \mathbf{u} + \rho \mathbf{g}, \\ \nabla \cdot \mathbf{u} &= 0, \quad \frac{\partial T}{\partial t} + \mathbf{u} \cdot \nabla T = k_T \nabla^2 T, \end{aligned} \quad (2.1)$$

where  $\mathbf{u}$ ,  $p$ , and  $T$  are the fluid velocity, fluid pressure, and fluid temperature, respectively, at a point  $(x, y, z)$  inside the fluid layer, at time  $t$ ;  $\mathbf{g} = (0, 0, -g)$  is the acceleration due to gravity;  $\rho_0$  is the fluid density at a reference temperature  $T_1$ ;  $\rho$  and  $\eta$  are the density and the dynamic viscosity of the fluid, respectively, at a temperature  $T$ ;  $k_T$  is the thermal diffusivity. The fluid density  $\rho$  is a function of  $T$  in general and it is given by the linear expression  $\rho = \rho_0 \{1 - \alpha(T - T_1)\}$ , where  $\alpha$  is the coefficient of volume expansion. The boundary conditions for the velocity field are

$$\frac{\partial \mathbf{u}}{\partial z} \cdot \hat{i} = \frac{\partial \mathbf{u}}{\partial z} \cdot \hat{j} = \mathbf{u} \cdot \hat{k} = 0 \quad \text{at } z = 0, d.$$

The temperatures of the lower and upper boundaries of the fluid layer are modulated about their mean values  $T_1$  and  $T_2$ , respectively, such that the boundary conditions for the temperature field  $T$  are

$$T = \begin{cases} T_1 - \epsilon_0 \cos(\omega_0 t) & \text{at } z = 0, \\ T_2 + \epsilon_0 \cos(\omega_0 t) & \text{at } z = d, \end{cases}$$

where  $\omega_0 > 0$  and  $\epsilon_0 > 0$ , are the frequency and amplitude of modulation, respectively.

The system of equations (2.1) describes a basic state of rest given by

$$\begin{aligned} \mathbf{u}_0 &= \mathbf{0}, \quad p_0 = \rho_0 g \int \{1 - \alpha(T_0 - T_1)\} dz, \\ T_0 &= T_1 + \frac{T_2 - T_1}{d} z + \epsilon_0 \operatorname{real} \left[ \frac{\sinh\{(z/d - 1/2)\lambda\}}{\sinh(\lambda/2)} \exp(i\omega_0 t) \right], \end{aligned} \quad (2.2)$$

where  $\lambda = (i\omega_0 d^2 / k_T)^{1/2}$ .

### 3. Analysis

We make the variables in the governing equations (2.1) dimensionless, using  $d$  as the distance scale,  $d^2/k_T$  as the time scale, and  $\gamma d$  ( $\gamma = -(T_2 - T_1)/d$ ) as the temperature scale. During the nondimensionalization process, the Rayleigh number  $\text{Ra} = \gamma \alpha d^4 g / (k_T \nu)$  which is the dimensionless measure of the temperature gradient across the fluid layer, and the Prandtl number  $\sigma = \nu / k_T$ , appear as dimensionless parameters. Considering small perturbations in the basic state (2.2) in the form

$$\mathbf{u} = \frac{k_T}{d} (u, v, w), \quad p = p_0 + \left( \frac{\rho_0 k_T^2}{d^2} \right) p_1, \quad T = T_0 + d\gamma\theta,$$

we obtain the linearized system of partial differential equations satisfied by  $w$  and  $\theta$ :

$$\nabla^2 \frac{\partial w}{\partial t} = \sigma \nabla^4 w - \sigma \text{Ra} \left( \frac{\partial^2}{\partial z^2} - \nabla^2 \right) \theta, \tag{3.1}$$

$$\frac{\partial \theta}{\partial t} = -\frac{1}{\gamma d} \frac{\partial T_0}{\partial z} w + \nabla^2 \theta. \tag{3.2}$$

The boundaries are assumed to be stress-free. The boundary conditions are  $w = \theta = 0$  at  $z = 0, 1$ .

To solve the system of differential equations (3.1) and (3.2), we express  $w$  and  $\theta$  in terms of suitable eigenfunctions such that

$$(w, \theta) = \sum_{\ell=1}^N (A_\ell(t), B_\ell(t)) \sin(\ell\pi z) \exp\{i(k_1 x + k_2 y)\}, \tag{3.3}$$

where  $N$  is a positive integer. Multiplying (3.1) and (3.2) throughout by  $\sin(j\pi z)$ , and integrating under the limits of  $z$ , we obtain

$$\sum_{\ell=1}^N (k^2 + \ell^2 \pi^2) \delta_{\ell j} \dot{A}_\ell = - \sum_{\ell=1}^N \sigma (k^2 + \ell^2 \pi^2)^2 \delta_{\ell j} A_\ell + \sigma \text{Ra} k^2 \sum_{\ell=1}^N \delta_{\ell j} B_\ell, \tag{3.4}$$

$$\sum_{\ell=1}^N \delta_{\ell j} \dot{B}_\ell = \sum_{\ell=1}^N \{\delta_{\ell j} - 2\epsilon \text{real}[P_{j\ell} \exp(i\omega t)]\} A_\ell - \sum_{\ell=1}^N (k^2 + \ell^2 \pi^2) \delta_{\ell j} B_\ell, \tag{3.5}$$

for each  $j = 1, 2, 3, \dots, N$ , where  $k = (k_1^2 + k_2^2)^{1/2}$ ,  $\delta_{\ell j}$  is the Kronecker delta,  $\epsilon = \epsilon_0/(\gamma d)$ ,  $\omega = \omega_0 d^2/k_T$ , and

$$P_{\ell j} = \frac{\lambda}{\sinh(\lambda/2)} \int_0^1 \cosh\{(z - 1/2)\lambda\} \sin(\ell\pi z) \sin(j\pi z) dz.$$

The system of equations (3.4) and (3.5) can be represented in the form of a matrix differential equation given by

$$\mathcal{A} \dot{\mathbf{X}} = \mathcal{B} \mathbf{X}, \quad \det \mathcal{A} \neq 0, \tag{3.6}$$

where  $\mathcal{A}$  and  $\mathcal{B}$  are the respective coefficient matrices in (3.4) and (3.5) and

$$\mathbf{X} = (A_1 \ A_2 \ \dots \ A_N \ B_1 \ B_2 \ \dots \ B_N)',$$

where the symbol  $'$  denotes the matrix transpose. The system (3.6) has been found to be reasonably stiff so that Runge–Kutta methods are not suitable for integrating it numerically, because these methods take a huge amount of time for numerical computation. To deal with a stiff system, we have used another numerical integration technique which is been explained in brief in the next section and works well with the present problem.

**3.1. Floquet analysis** The periodic, homogeneous system (3.6) of ordinary differential equations can be solved using Floquet analysis [6, 8]. The details of the numerical method employed are given in the references [6, 11]. For the eigenfunction expansions (3.3), we take  $N = 3$ . The interval  $[0, 2\pi/\omega]$  is divided into  $m$  equal parts by  $t_0 = 0 < t_1 < t_2 < \dots < t_m = 2\pi/\omega$ , such that each subinterval  $[t_{j-1}, t_j]$ ,  $j = 1, 2, \dots, m$ , has length  $h = 2\pi/(\omega m)$ .

Let  $\mathbf{F}(t) = \mathcal{A}(t)^{-1} \mathcal{B}(t)$ . Then  $\mathbf{F}(t_{j-1} + t) \approx \mathbf{F}(t_{j-1})$ , for all  $t \in [t_{j-1}, t_j]$ , for  $h$  sufficiently small. Let  $\Phi(t)$  denote a fundamental matrix for the regular system (3.6). Its value at  $t = t_j$  is approximated by

$$\Phi(t_j) = \Phi(t_{j-1}) \exp\{h\mathbf{F}(t_{j-1})\}. \quad (3.7)$$

Using this iteration scheme, the approximate solution at  $t = 2\pi/\omega$  is found to be

$$\Phi(2\pi/\omega) = \Phi(0) \exp\{h\mathbf{F}(0)\} \exp\{h\mathbf{F}(h)\} \exp\{h\mathbf{F}(2h)\} \dots \exp\{h\mathbf{F}((m-1)h)\},$$

where we take  $\Phi(0) = \mathbf{I}$  as the identity matrix of order  $2N$ . The eigenvalues of  $\Phi(2\pi/\omega)$  are the Floquet multipliers. The Floquet exponents  $\lambda_j$  and the Floquet multipliers  $\mu_j$  are related by  $\mu_j = \exp(2\pi\lambda_j/\omega)$ ,  $1 \leq j \leq 2N$ .

The  $\mu_j$  and hence  $\lambda_j$  terms are functions of the dimensionless parameters: the modulation frequency  $\omega$ , the modulation amplitude  $\epsilon$ , the Rayleigh number  $Ra$ , the Prandtl number  $\sigma$ , and the wavenumber  $k$ .

The marginal state of the modulated system is determined by setting

$$\max_{1 \leq j \leq 2N} \{\text{real}(\lambda_j)\} = 0. \quad (3.8)$$

The basic modulated flow is stable for  $\max_{1 \leq j \leq 2N} \{\text{real}(\lambda_j)\} < 0$ , and unstable for  $\max_{1 \leq j \leq 2N} \{\text{real}(\lambda_j)\} > 0$ . If a Floquet exponent satisfying (3.8) is identically zero, then the disturbance in the marginal state oscillates periodically with the forcing frequency  $\omega$ , and the instability response is called synchronous or harmonic. On the other hand, if the imaginary part of the Floquet exponent satisfying (3.8) is equal to  $\omega/r$ , for some positive integer  $r > 1$ , the disturbance in the marginal state oscillates with a frequency  $\omega/r$ , and the instability response is called subharmonic of order  $1/r$ .

Considering again the system of equations (3.4) and (3.5), we write the coefficients  $A_\ell(t)$  and  $B_\ell(t)$  in terms of the truncated Fourier series

$$(A_\ell(t), B_\ell(t)) = \sum_{q=-L}^L (A_{\ell q}, B_{\ell q}) \exp\{(s + iq\omega)t\},$$

where  $L$  is a positive integer and  $s$  is the Floquet exponent.

The system of equations (3.4) and (3.5) now satisfies

$$\mathbf{H}_q \Theta_q = \epsilon (\mathbf{Q} \Theta_{q-1} + \bar{\mathbf{Q}} \Theta_{q+1}), \quad (3.9)$$

for each  $q = -L, -L + 1, \dots, 0, \dots, L - 1, L$ . Here,

$$\Theta_q = (A_{1q} \ A_{2q} \ \cdots \ A_{Nq} \ B_{1q} \ B_{2q} \ \cdots \ B_{Nq})', \quad \mathbf{H}_q = \begin{pmatrix} \mathbf{A}_q & \mathbf{D} \\ \mathbf{C} & \mathbf{B}_q \end{pmatrix}, \quad \mathbf{Q} = \begin{pmatrix} \mathbf{0} & \mathbf{0} \\ \mathbf{P} & \mathbf{0} \end{pmatrix},$$

where

$$\mathbf{A}_q = -(a_{\ell q} \delta_{\ell j})_{N \times N}, \quad \mathbf{B}_q = -(b_{\ell q} \delta_{\ell j})_{N \times N}, \quad \mathbf{C} = (\delta_{\ell j})_{N \times N}, \\ \mathbf{D} = \sigma \text{Ra} \ k^2 (\delta_{\ell j})_{N \times N}, \quad \mathbf{P} = (P_{\ell j})_{N \times N},$$

and  $\mathbf{0}$  denotes the zero matrix of order  $N$ . The elements  $a_{\ell q}$  and  $b_{\ell q}$  are given by

$$a_{\ell q} = \left( k^2 + \ell^2 \pi^2 \right) (s + iq\omega) + \sigma \left( k^2 + \ell^2 \pi^2 \right)^2, \quad b_{\ell q} = s + iq\omega + k^2 + \ell^2 \pi^2.$$

Equation (3.9) leads to the eigenvalue problem given by

$$\mathbf{TZ} = \epsilon \mathbf{UZ}, \quad \det \mathbf{T} \neq 0, \quad (3.10)$$

where  $\mathbf{T}$  and  $\mathbf{U}$  are the coefficient matrices related to (3.9) such that it is equivalent to the representation (3.10) and  $\mathbf{Z} = (\Theta'_{-L}, \Theta'_{-L+1}, \dots, \Theta'_{L-1}, \Theta'_L)'$ .

The eigenspectrum of the linear operator  $\mathbf{T}^{-1}\mathbf{U}$  in (3.10) consists of the values of  $1/\epsilon$ ,  $\epsilon \neq 0$ . The real positive values of  $\epsilon$  can be calculated by numerically evaluating the eigenspectrum of  $\mathbf{T}^{-1}\mathbf{U}$  as a function of the dimensionless parameters.

#### 4. Results and discussion

The fundamental matrix  $\Phi(2\pi/\omega)$  is obtained using the recurrence relation (3.7). A reduced step size  $h$  is required to obtain high accuracy as the modulation amplitude  $\epsilon$  increases. To check the correctness of the numerical results obtained by the present integration technique, we carried out numerical integration of the system (3.6) to obtain the critical Rayleigh number for a typical value of  $\epsilon = 10$ ; the other parametric values are taken as  $\sigma = 0.73$  and  $\omega = 20$ . Letting  $m$  denote an approximate minimum number of points of evaluation required for convergence of a numerical method over one time period, then  $h = 2\pi/(\omega m)$ . The  $\text{Ra}_c$  values obtained by solving (3.6), using the present method are compared in Table 1 with those obtained by employing the powerful Runge–Kutta methods of integration, namely, the Runge–Kutta–Fehlberg method (RKF45), the fourth-order Runge–Kutta method (RK4), and the Runge–Kutta–Gill procedure (RKG) (see Table 1).

From Table 1 we see that the various methods converge to almost same value of  $\text{Ra}_c$ . The number of points of evaluation for the convergence of Runge–Kutta methods is very small compared to the number of points of evaluation required by the present method. However, it has been found that the Runge–Kutta methods take a great deal of time to obtain the velocity and temperature profiles (where it is necessary to use a particular method repeatedly) even if  $m$  is taken small, whereas the present method

TABLE 1. Critical Rayleigh number  $Ra_c$  and corresponding wavenumber  $k_c$  as obtained using different numerical integration techniques for  $\epsilon = 10$ ,  $\sigma = 0.73$  and  $\omega = 20$ .

$N$	Present method $m$	RK45 $m$	RK4 $m$	RKG $m$	$k_c$	$Ra_c$
8	3000	132	360	360	3.47	305.5038
7	3000	132	360	360	3.47	305.5038
6	3000	151	431	431	3.47	305.5038
5	3000	151	431	431	3.47	305.5038
4	3000	153	431	431	3.47	305.4998
3	3000	153	431	431	3.47	305.4998
2	3000	153	431	431	3.46	303.4753
1	3000	153	431	431	3.46	303.4753

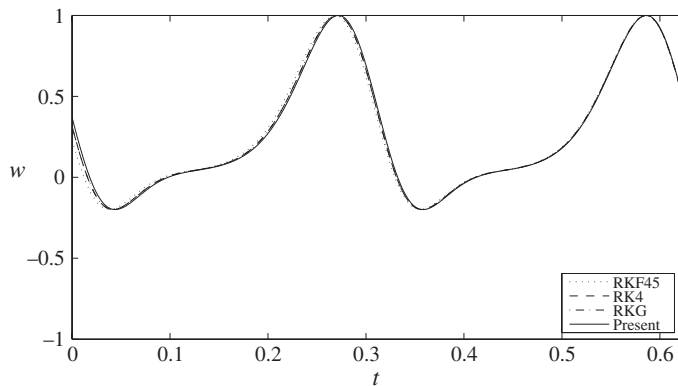


FIGURE 1. Normalized vertical velocity profile at the onset of harmonic flow for two time periods as predicted by the various numerical integration methods for  $\epsilon = 10$ ,  $N = 3$ ,  $\sigma = 0.73$ ,  $w = 20$ .

works faster even when  $m$  is quite high. Figures 1 and 2 demonstrate the normalized velocity and temperature profiles as depicted by the various numerical integration methods for  $N = 3$ , which are practically indistinguishable.

The normalized velocity profile for  $w$  is not affected by increasing  $N$ , but the normalized temperature profile for  $N = 1$  has been found to be different from those drawn at higher  $N$  (Figures 3 and 4). Nevertheless the shape of the profile remains unaltered in all the cases. We have seen that  $N = 3$ , along with  $m \geq 3000$ , is sufficient to obtain the correct profiles by employing the present numerical integration technique, for  $\epsilon$  values not exceeding 10.

It has been found numerically that the critical state oscillates time periodically, either with the natural frequency or with half of the natural frequency of modulation. Figure 5 illustrates a variation of critical Rayleigh number  $Ra_c$  with the amplitude of

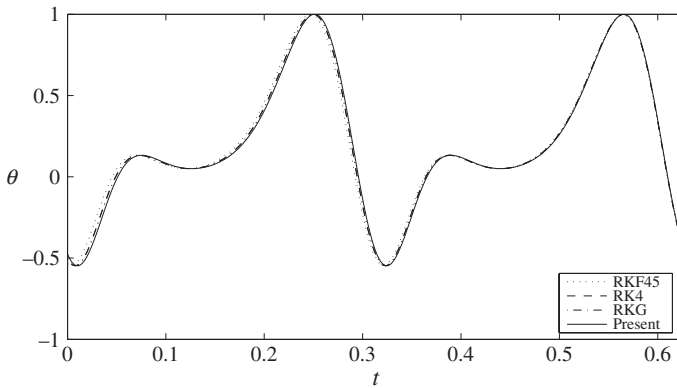


FIGURE 2. Normalized temperature profile at the onset of harmonic flow for two time periods as predicted by the various numerical integration methods for  $\epsilon = 10$ ,  $N = 3$ ,  $\sigma = 0.73$ ,  $\omega = 20$ .

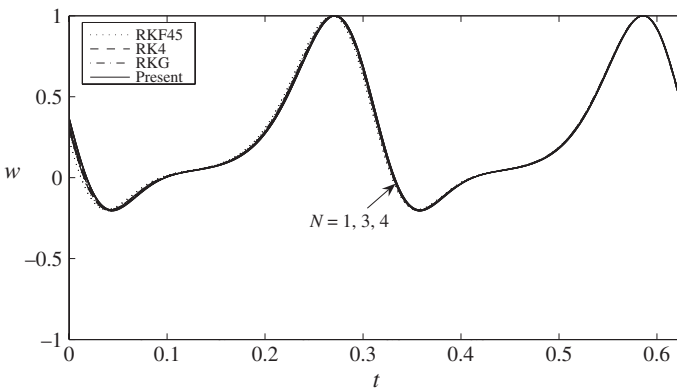


FIGURE 3. Normalized vertical velocity profile at the onset of harmonic flow for two time periods as predicted by the various numerical integration methods for different values of  $N$  at  $\epsilon = 10$ ,  $\sigma = 0.73$ ,  $\omega = 20$ .

modulation  $\epsilon$ , for the Prandtl number of air (0.73). For  $\epsilon = 0$  (that is, in the absence of temperature modulation), the Rayleigh–Bénard convection starts at  $Ra = 657.51$ . With an increase in modulation amplitude, the onset of convection is delayed. For  $\epsilon \geq 1.2$ , subharmonic instability appears. The critical value of the Rayleigh number for the onset of subharmonic instability decreases with an increase in the amplitude of modulation. When  $\epsilon$  exceeds approximately 2.1, the critical Rayleigh number falls below its value corresponding to no modulation.

The streamline patterns at the onset of instability as harmonic flow and subharmonic flow are shown in the  $(y, z)$  plane in Figures 6 and 7, respectively. The roll patterns extending periodically in the  $y$  direction are evident from the figures. The flow alternates between the adjacent rolls. The cell size in each roll is comparatively smaller in the case of harmonic flow.

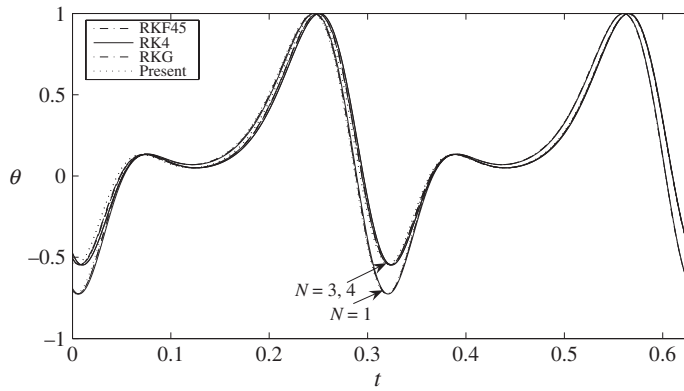


FIGURE 4. Normalized temperature profile at the onset of harmonic flow for two time periods as predicted by the various numerical integration methods for different values of  $N$  at  $\epsilon = 10$ ,  $\sigma = 0.73$ ,  $\omega = 20$ .

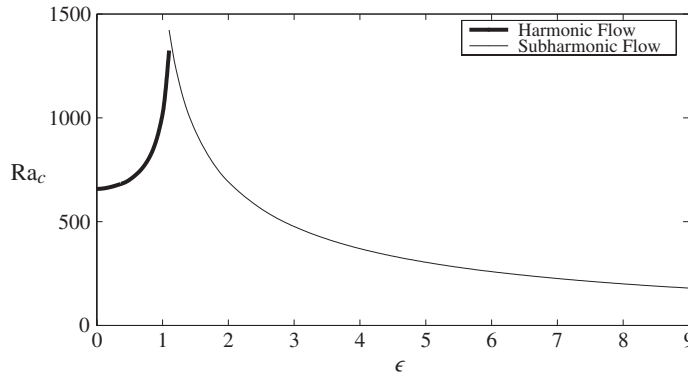


FIGURE 5. Critical curve in  $(\epsilon, Ra_c)$  plane at  $\sigma = 0.73$  and  $\omega = 20$ .

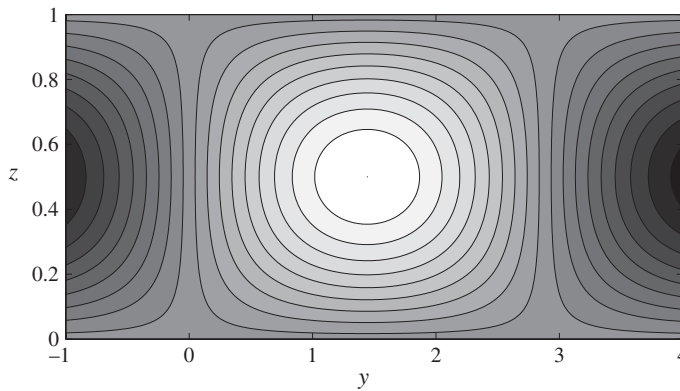


FIGURE 6. Cell pattern in  $(y, z)$  plane at the onset of harmonic for  $\epsilon = 1.1$ ,  $Ra = 1324$  and  $\sigma = 0.73$ .

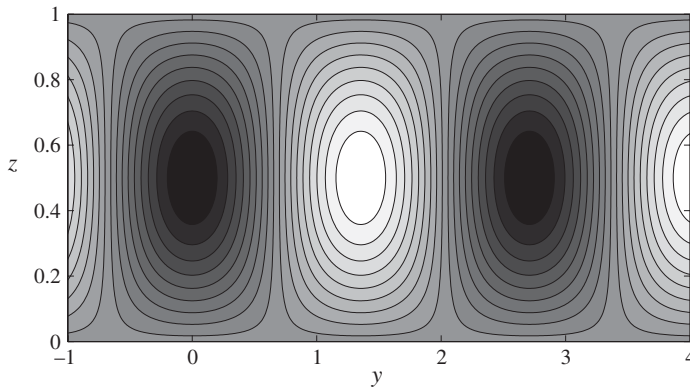


FIGURE 7. Cell pattern in  $(y, z)$  plane at the onset of subharmonic flow for  $\epsilon = 1.1$ ,  $Ra = 1423$  and  $\sigma = 0.73$ .

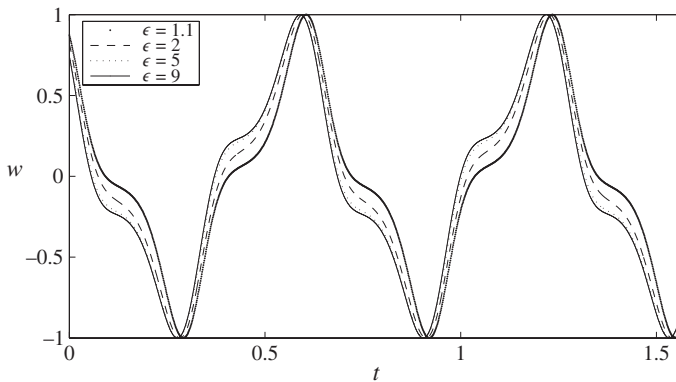


FIGURE 8. The normalized  $z$  component of the velocity field perturbation at the onset of subharmonic flow for  $\sigma = 0.73$  and  $\omega = 20$ .

The normalized velocity field  $w$  at the critical onset of convection is shown with respect to  $t$  in Figure 8 for different values of the amplitude of modulation. The profiles have been drawn for  $0 \leq t \leq 10\pi/\omega$  and  $z = 1/2$ . The fluctuations in  $w$  increase with an increase in modulation amplitude. Observe that  $w$  can be negative, zero, or positive with increase in  $t$ . A similar variation (not shown here) occurs in the normalized profiles for the  $x$  and  $y$  components of the velocity field perturbations.

The time evolution of the corresponding normalized temperature field  $\theta$  is illustrated in Figure 9. It is interesting to note that there is a time lag between the corresponding extreme values of  $w$  and  $\theta$ , the former lagging behind the latter. This is due to the counter-action of the inertia of the fluid carried by the disturbance  $w$  which acts so as to oppose the change of flow direction. Figures 10 and 11 illustrate the time evolution of the normalized  $z$  component of the velocity field and the temperature field, respectively, at the critical onset of convection for  $0 \leq t \leq 10\pi/\omega$  and  $z = 1/2$ .

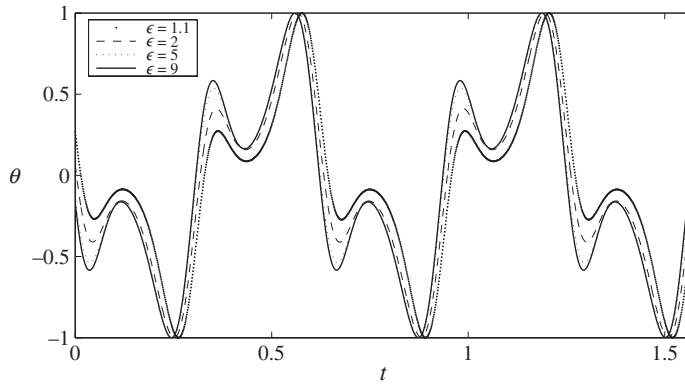


FIGURE 9. Normalized temperature profile at the onset of subharmonic flow for  $\sigma = 0.73$  and  $\omega = 20$ .

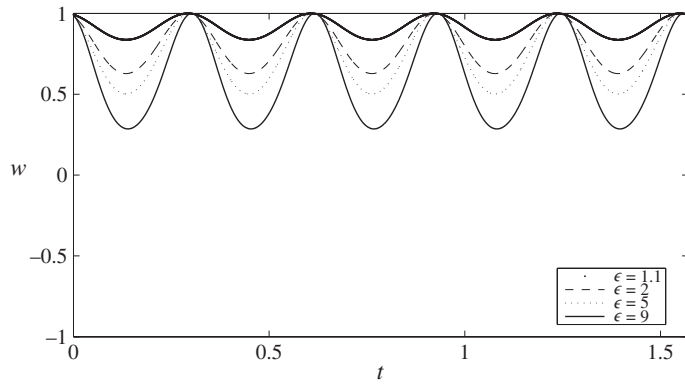


FIGURE 10. Normalized  $z$  component of the velocity field perturbation at the onset of harmonic flow for  $\sigma = 0.73$  and  $\omega = 20$ .

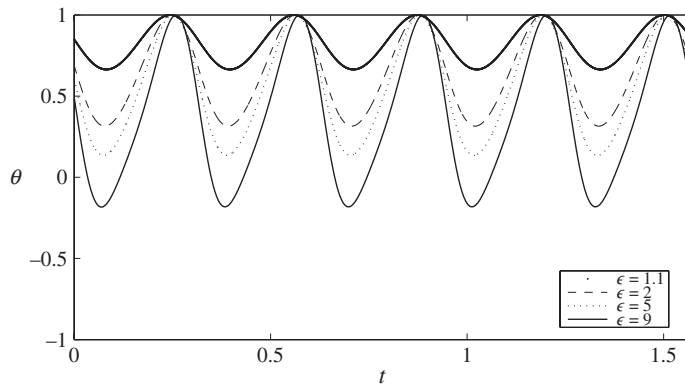


FIGURE 11. Normalized temperature profile at the onset of harmonic flow for  $\sigma = 0.73$  and  $\omega = 20$ .

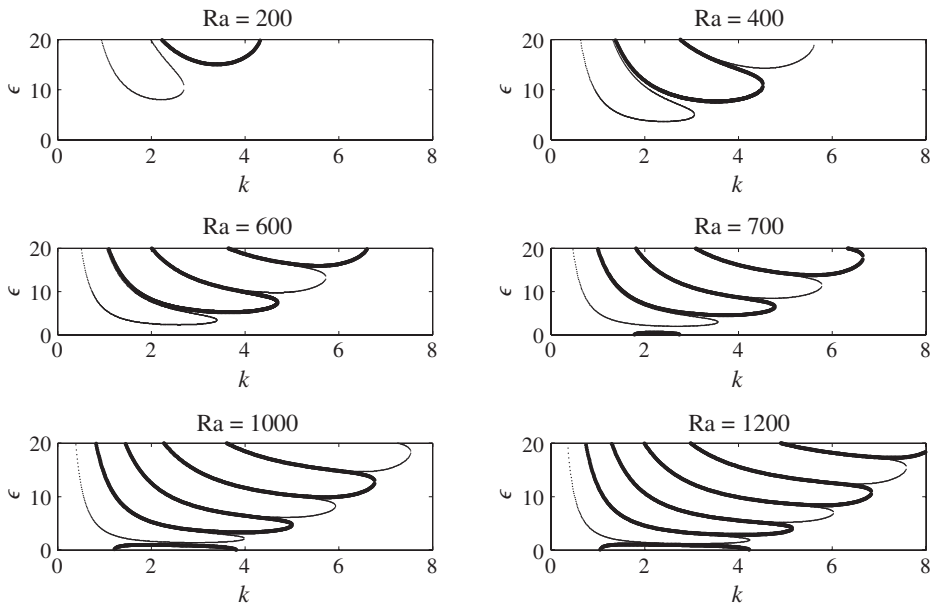


FIGURE 12. Resonance bands in the  $(k, \epsilon)$  plane for  $\sigma = 0.73$  and  $\omega = 20$ .

In the eigenvalue problem (3.10), the reciprocal of an eigenvalue of  $\mathbf{T}^{-1}\mathbf{U}$  gives the amplitude of modulation for the onset of instability. The eigenvalue  $1/\epsilon$  is a function of the Rayleigh number  $Ra$ , the Prandtl number  $\sigma$ , the modulation frequency  $\omega$ , and the wavenumber of disturbance  $k$ . For calculation purposes, we fix the value of the Floquet exponent  $s$  equal to zero to obtain the results for the synchronous mode and  $s = 1/2$  for the subharmonic mode of instability. The resonance bands in the  $(k, \epsilon)$  plane have been obtained using  $L = 12$  and  $N = 3$ . The eigenvalues of the fundamental matrix give the Floquet multipliers.

We obtain numerically the values of  $\epsilon$  in a range of  $k$ , for various values of the Rayleigh number, Prandtl number, and forcing frequency. Instability zones in the form of tongues are observed. Figure 12 shows the pattern of instability zones at various values of  $Ra$ , for fixed parametric values  $\sigma = 0.73$  and  $\omega = 20$ . The points on each band correspond to harmonic or subharmonic instability. Within a particular tongue the basic state is unstable, and outside the tongue the basic state is stable. The darker points in the figure correspond to harmonic instability and lighter points correspond to subharmonic instability. Alternate harmonic and subharmonic resonance bands appear for different Rayleigh numbers. The fundamental region of instability appears for  $Ra$  exceeding its critical value corresponding to convection in the absence of modulation, that is,  $Ra_c = 657.511$ . For  $Ra > Ra_c$ , the system is unstable without temperature modulation. The fundamental mode of instability can be stabilized with sinusoidal modulation of boundary temperatures; however, this stabilization is bounded above by

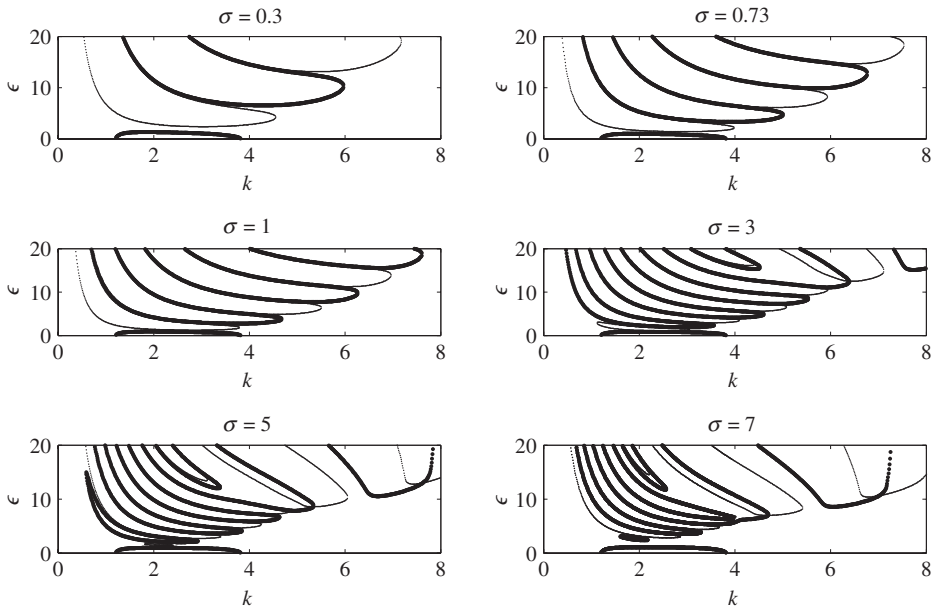


FIGURE 13. Instability zones in the  $(k, \epsilon)$  plane for  $Ra = 1000$  and  $\omega = 20$ .

the resonant instability zones. As the Rayleigh number increases, the resonance bands become narrower. However, the number of bands increases in the region considered.

It has been observed that at a fixed Rayleigh number, the instability regions are affected by increasing the Prandtl number. This variation is evident from Figure 13. The instability zones become narrower with an increase in  $\sigma$ . The synchronous and subharmonic modes of instability alternate with an increase in the Prandtl number. However, at a subcritical Rayleigh number  $Ra = 300$ , the resonance bands may shift upwards or downwards along the  $\epsilon$  axis, depending upon the Prandtl number (Figure 14). The instability zones also shift towards the higher wavenumber, indicating that the convection cells will become narrower for higher Prandtl numbers.

We have also observed the resonance bands in the  $(k, \epsilon)$  space for various values of the modulation frequency  $\omega$  (see Figure 15). At  $\omega = 5$ , the resonance bands are densely packed, and overlapping between some of them also occurs. The density of the packing decreases gradually when the frequency is increased. Observe that the fundamental region also rises with an increase in  $\omega$ . Thus, a higher amplitude of modulation is needed to stabilize the fundamental mode of Rayleigh–Bénard convection at higher frequencies. At or above  $\omega = 40$ , we observe that only one tongue remains above the fundamental region in the range of  $k$  and  $\epsilon$  considered, which corresponds to subharmonic instability. The pattern shows that an increase in the modulation frequency suppresses the onset of a periodic flow.

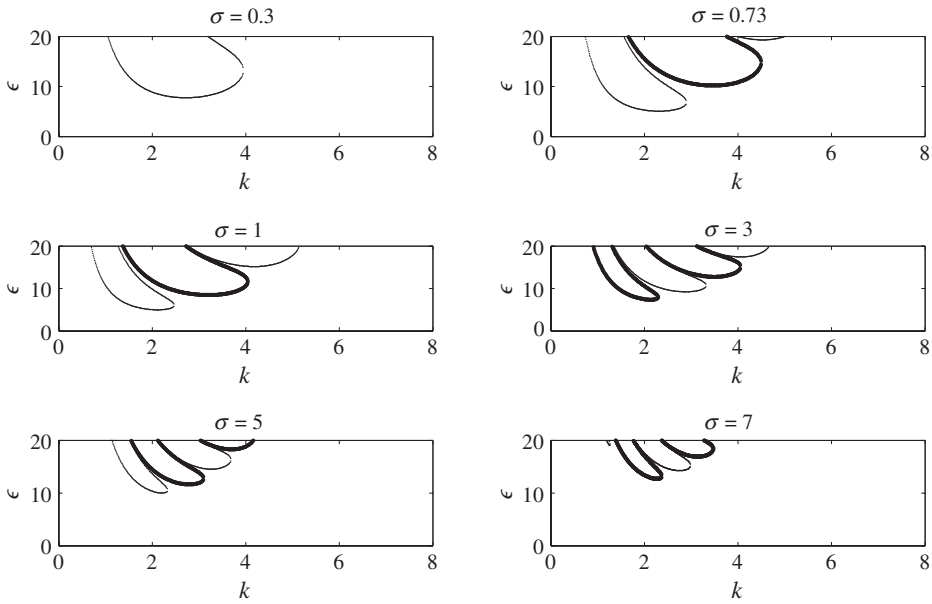


FIGURE 14. Instability zones in the  $(k, \epsilon)$  plane for  $Ra = 300$  and  $\omega = 20$ .

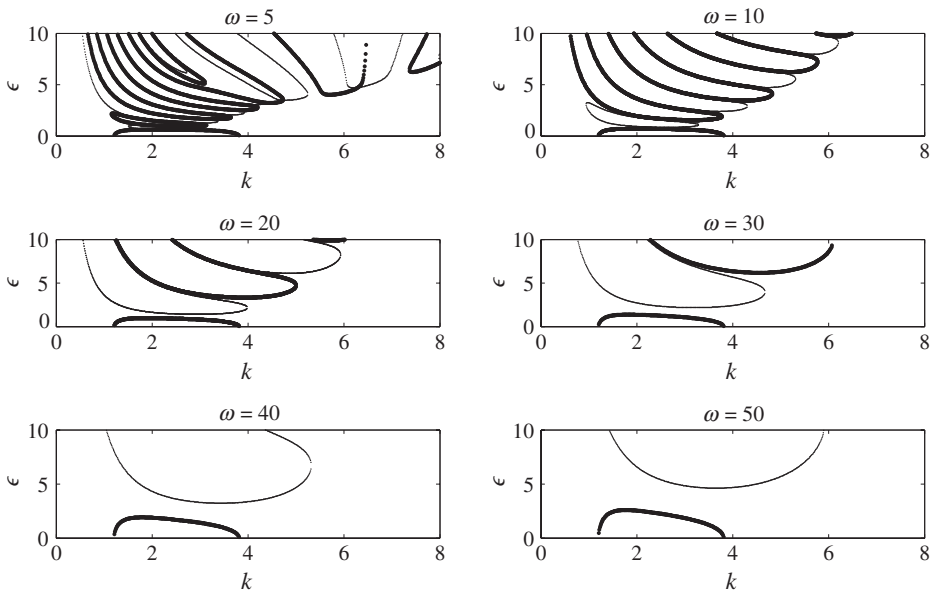


FIGURE 15. Resonance bands in the  $(k, \epsilon)$  space for  $Ra = 1000$  and  $\sigma = 0.73$ .

## 5. Concluding remarks

The effect of time periodic modulation of the free-boundary temperatures in the Rayleigh–Bénard convection of an infinite, horizontal, Boussinesq fluid layer has been studied numerically using Floquet theory. The critical onset of convection can be a time-periodic harmonic or subharmonic flow, depending upon modulation.

Modulation can cause the convection to occur even in the subcritical Rayleigh numbers. Also, the presence of modulation can suppress the convection in the supercritical flow regime. In the presence of modulation, an increase in the Rayleigh number has a tendency to advance the onset of periodic flows, while an increase in the Prandtl number and the modulation frequency oppose this effect. Thus, with the proper tuning of the parameters, the onset of convection in the form of periodic flows can be controlled. These results may be helpful in giving some insight into understanding and controlling the instability phenomena driven by temperature modulation in the real physical situations where the natural convection occurs.

## References

- [1] R. Bajaj, “Thermo-magnetic convection in ferrofluids with gravity-modulation”, *Indian J. Eng. Mater. Sci.* **10** (2002) 282–291.
- [2] E. Bodenschatz, W. Pesch and G. Ahler, “Recent developments in Rayleigh–Bénard convection”, *Annu. Rev. Fluid Mech.* **32** (2000) 709–778.
- [3] S. Chandrasekhar, *Hydrodynamic and hydromagnetic stability* (Oxford University Press, Oxford, 1966).
- [4] W. Y. Chen and C. F. Chen, “Effect of gravity modulation on the stability of convection in a vertical slot”, *J. Fluid Mech.* **395** (1999) 327–344.
- [5] P. Drazin and W. Reid, *Hydrodynamic stability* (Cambridge University Press, Cambridge, 1981).
- [6] M. Farkas, *Periodic motions* (Springer-Verlag, New York, 1994).
- [7] P. M. Gresho and R. L. Sani, “The effect of gravity modulation on the stability of a heated fluid layer”, *J. Fluid Mech.* **40** (1970) 783.
- [8] D. W. Jordan and P. Smith, *Nonlinear ordinary differential equations* (Clarendon Press, Oxford, 1988).
- [9] E. L. Koschmieder, *Bénard cells and Taylor vortices* (Cambridge University Press, Cambridge, 1993).
- [10] K. Kumar, “Linear theory of Faraday instability in viscous liquids”, *Proc. R. Soc. Lond. A* **452** (1994) 1113–1126.
- [11] E. Nelson, *Topics in dynamics I: flows* (Princeton University Press and University of Tokyo Press, Princeton, NJ, 1969).
- [12] M. N. Roppo, S. H. Davis and S. Rosenblat, “Bénard convection with time-periodic heating”, *Phys. Fluids* **27** (1984) 796–803.
- [13] S. Rosenblat and G. A. Tanaka, “Modulation of thermal convection instability”, *Phys. Fluids* **14** (1971) 1319–1322.
- [14] G. Venezian, “Effect of modulation on the onset of thermal convection”, *J. Fluid Mech.* **395** (1999) 327–344.
- [15] C. S. Yih and C. H. Li, “Instability of unsteady flows or configurations. Part 2. Convective instability”, *J. Fluid Mech.* **54** (1972) 143–152.